CHALMERS

Frequency Sweeping Directivity of Bursting Alfvén Waves on MAST

Master of Science Thesis in the Master Degree Programme, Fundamental Physics

FRIDA HÅKANSSON

Department of Earth and Space Sciences
Nonlinear Electrodynamics
CHALMERS UNIVERSITY OF TECHNOLOGY
Gothenburg, Sweden, 2012

Frequency Sweeping Directivity of Bursting Alfvén Waves on MAST

Frida Håkansson

CHALMERS

Department of Earth and Space Sciences
Chalmers University of Technology
Göteborg, Sweden 2012

Frequency Sweeping Directivity of Bursting Alfvén Waves on MAST
Frida Håkansson

Department of Earth and Space Sciences
Nonlinear Electrodynamics
Chalmers University of Technology
SE-412 96 Göteborg, Sweden
Telephone +46 (0)31-772 1000

Chalmers Reproservice
Göteborg, Sweden 2012

Frequency Sweeping Directivity of Bursting Alfvén Waves on MAST

Frida Håkansson
Department of Earth and Space Sciences
Chalmers University of Technology
SE-412 96 Göteborg, Sweden

Abstract

In a burning plasma, such as the next generation tokamak experiment ITER, significant numbers of highly energetic alpha particles will be produced. The presence of energetic particles may excite kinetic instabilities and affect the transport and heating of particles in the plasma. Of particular interest is the so called toroidal Alfvén eigenmode (TAE) which can be excited by the super Alfvénic alpha particles through resonant wave-particle interaction. In this thesis we identfy the linear TAEs with corresponding bursting nonlinear evolution in a discharge on the spherical tokamak MAST using the equilibrium code HELENA and the linear codes CSCAS and MISHKA. If this mode is excited there is a consecutive exponential growth of the linearized perturbations when the linear growth rate due to the fast particles is slightly larger then the total damping in the plasma. Nonlinear theory is then needed to describe the evolving nonlinear modes, which are observed to sweep in frequency with a preferred frequency sweeping directivity that changes in time. We investigate a possible reason for the change in preferred frequency sweeping directivity and derive an expression for the radial motion of the mode during the frequency sweeping.

Keywords: Fusion plasma physics, toroidal Alfvén eigenmode, wave-particle interaction, linear growth rate, frequency sweeping

Contents

1

Introduction

Throughout the world there is a steadily increasing demand for energy production, more than what the current energy sources can provide for in an economically feasible and environmentally friendly manner [1]. From an environmental point of view, there are limits to how much energy can be supplied from fossil fuels such as oil and coal. Together with the increasing energy demand in the world it is clear that there is a necessity for new environmentally friendly energy sources. This is where fusion comes in.

Thermonuclear fusion is the energy source of the stars. It is the process where two nuclei merge to one nuclei which has a lower binding energy and therefore energy is released. The candidates for fusion energy production here on Earth involves the hydrogen isotopes deuterium (D) and tritium (T) in the following reactions:

$$\mathrm{D} + \mathrm{D} \longrightarrow \mathrm{He}^3 + n + 3.27 \text{ MeV} \tag{1.1a}$$

$$\mathrm{D} + \mathrm{D} \longrightarrow \mathrm{T} + \mathrm{H} + 4.05 \text{ MeV} \tag{1.1b}$$

$$\mathrm{D} + \mathrm{T} \longrightarrow \mathrm{He}^4 + n + 17.58 \text{ MeV} \tag{1.1c}$$

The reaction probability and energy output is highest for the D-T reaction. The temperature required for this reaction is approximately 10^8 K. At these temperatures the gas is completely ionised and is known as a *plasma*. To use thermonuclear fusion as an energy source there are some problems that need to be overcome. One problem is the confinement of the plasma. In stars, confinement of the particles is provided by gravitation. Here on Earth, the current main schemes are inertial fusion and magnetic confinement. Inertial fusion is the compressing and heating of a capsule of D-T by uniform radiation from a laser. An outer layer evaporates with a resulting implotion of the capsule that creates the condition for fusion to occur. Magnetic confinement

is currently the most promising confinement scheme and uses the basic fact that a plasma consists of charged particles which follow magnetic field lines. The problem is the design of magnetic field topology for the confinement.

Tokamaks [2] are axisymmetric, toroidal configurations which confine plasma particles through the use of an externally generated toroidal magnetic field with a smaller poloidal magnetic field generated inside the device by running currents through the plasma. There is a large number of tokamak experimental facilities operating or being constructed, the largest currently in operation is the Joint European Torus (JET), see Figure (1.1). Spherical tokamaks, like MAST (Mega Ampere Spherical Tokamak), see Figure (1.2), are small, fat tokamaks with a large ratio of minor to major radius. This geometry allows it to operate with a high ratio of particle to magnetic pressure but also puts a lower limit on the magnetic field strength, due to the narrow inner leg. The largest experimental tokamak facility, currently under construction, is the internationally funded facility ITER (International Thermonuclear Experimental Reactor) which will be almost twice the linear size of JET. ITER aims to demonstrate that it is possible to produce commercial energy from fusion [3]. The main objectives are: To momentarily produce ten times more thermal energy from fusion heating than is supplied by auxilary heating, i.e $Q = 10$. To produce a steady state plasma with $Q > 5$. To maintain a fusion pulse for up to eight minutes.

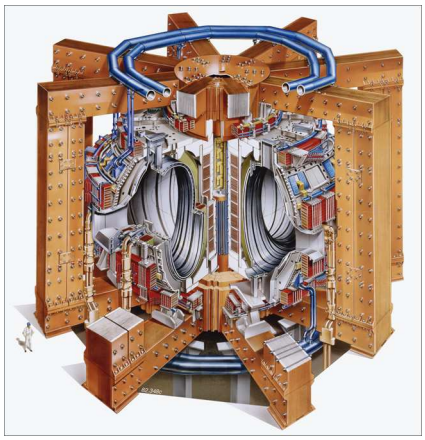

Figure 1.1: JET

Figure 1.2: MAST

The tokamak D-T plasmas are heated ohmically by a current in the plasma and from the fusion born alpha particles, but external heating schemes are also necessary, such as neutral beam injection (NBI) and radio frequency heating. NBI consists of a highly energetic beam of neutrals injected into the plasma where they are ionized and heat the plasma through collisions. Radio frequency

waves heat the plasma through resonant interaction between the waves and the plasma particles. The resulting fast particles, be it fusion born or injected into the plasma, are highly energetic with velocities exceeding the thermal velocity of ions in the plasma. Moreover, their velocities do not conform to a Maxwellian distribution function like the bulk plasma. Thus, the presence of fast particles provides free energy available to drive instabilities in the plasma [4]. These instabilites are mainly unwanted since they may degrade the plasma particle heating, cause alpha particle losses and damage the first wall.

The remainder of the thesis is organized as follows: In Chapter 2, we look at general properties of a plasma and investigate the motion of a single charged particle in a given magnetic field. We present the magnetohydrodynamic model which we use to look at the equilibrium and stability properties of a plasma. In Chapter 3, we consider toroidal systems. We investigate Alfvén waves and their behaviour in tokamaks, magnetohydrodynamic features such as the Alfvén continuum and its associated damping, toroidal Alfvén eigenmodes and excitation of modes by fast particles. We also present the possible nonlinear evolution of the fast particle induced instabilities and derive an expression for the radial motion of particles in a wave with time-dependent frequency. In Chapter 4 we identify the linear modes with corresponding bursting nonlinear evolution in a MAST discharge and propose a possible reason for the change in preferred frequency sweeping directivity of the nonlinear evolution.

2

Theoretical Description of a Plasma

A plasma is often thought of as a hot ionised gas whose behaviour is dominated by long-range electric and magnetic fields. One definition of a plasma is [5]:

> A plasma is a quasi-neutral gas consisting of charged and neutral particles exhibiting collective behaviour.

The keywords here are quasi-neutral and collective behaviour. Quasi-neutrality means that there may occur deviations from neutrality on a microscopic level, but the plasma is macroscopically neutral. Collective behaviour refers to the fact that a particle in a plasma interacts with a large number of other particles simultaneously. This, since the electrical force between charged particles is long range.

For the long range collective effects to dominate over short range Coulomb interactions and for the plasma to have the ability to screen out changes in the electric field certain conditions need to be fulfilled. To formulate these conditions we use a characteristic length scale, λ_D, called the *Debye length*

$$\lambda_D^2 \equiv \frac{\epsilon_0 k_B T_e}{n e^2} \ , \tag{2.1}$$

and a characteristic frequency of oscillations

$$\omega_p^2 = \frac{n e^2}{m_e \epsilon_0} \ , \tag{2.2}$$

called the *plasma frequency*. In these expressions ϵ_0 is the permittivity of free space, n is the plasma number density, k_B is the Boltzmann constant and e, m_e and T_e are the charge, mass and temperature of electrons, respectively.

The Debye length is the distance at which local, microscopic deviations from quasi-neutrality are effectively screened out, which must be small compared to the plasma dimensions in order to permit quasi-neutrality. Furthermore, to be able to use electromagnetic laws for the description of a plasma, collisions can not be too frequent. Note that the fact that a plasma effectively screens out the change in electric fields and that there are few Coulomb collisions imply a high conductivity. Finally, the number of particles in a sphere of radius λ_D need to be large for the statistical laws behind the distribution function to be valid. These conditions can be expressed as

$$\lambda_D \ll L \tag{2.3a}$$

$$\nu \ll \omega_p \tag{2.3b}$$

$$\frac{4\pi}{3}\lambda_D^3 n_0 \gg 1 \tag{2.3c}$$

where L is the macroscopic dimension of the plasma and ν is the collision frequency between charged particles. When a system fulfills (2.3) it is said to constitute a plasma.

When describing a plasma it is important to have a model that is able to describe the collective behaviour of particles and interaction between the particles and fields. The particles in the plasma interact with both internal fields produced by the particles themselves and with externally applied fields. This gives rise to nonlinear behaviour. Given the trajectory and velocity of each particle, the electric and magnetic field can be evaluated using the Maxwell equations

$$\nabla \times \mathbf{E} = -\frac{\partial \mathbf{B}}{\partial t} \ , \tag{2.4a}$$

$$\nabla \times \mathbf{B} = \mu_0 \epsilon_0 \frac{\partial \mathbf{E}}{\partial t} + \mu_0 \mathbf{J} \ , \tag{2.4b}$$

$$\nabla \cdot \mathbf{E} = \frac{\rho}{\epsilon_0} \ , \tag{2.4c}$$

$$\nabla \cdot \mathbf{B} = 0 \ , \tag{2.4d}$$

where $\mathbf{E}$ and $\mathbf{B}$ are the electric and magnetic field vectors, $\mathbf{J}$ is the current density vector, ρ is the charge density and μ_0 is the vacuum permeability. Simultaneously, given the instantaneous electric and magnetic field, the forces on each particle can be evaluated using the Lorentz force equation of motion

$$m\frac{d\mathbf{v}}{dt} = q(\mathbf{E} + \mathbf{v} \times \mathbf{B}) \ , \tag{2.5}$$

where $\mathbf{v}$, m and q are the velocity vector, mass and charge of the particle, respectively. This equation can then be used to update the trajectories and

velocities of particles. However, due to a large number of particles and complexity of the electromagnetic field this approach is impractical if not impossible. For instance, initial conditions for all the particles would be needed. Nevertheless, we can still gain some understanding by considering the motion of a single particle.

2.1 Single-Particle Motion

When considering the motion of a single charged particle in a plasma we will assume collisionless motion and will not include the currents and corresponding induced magnetic fields from the flow of charged particles. The resulting motion in a magnetized plasma will consist of a circulating motion, the Larmor gyration, superimposed on the so called guiding center motion which mainly follow the magnetic field lines, and slowly drifts across them.

2.1.1 Larmor Gyration

The equation of motion for a charged particle is the Lorentz force equation (2.5). With a homogeneous magnetic field, and in the absence of an electric field, it becomes

$$m\frac{d\mathbf{v}}{dt} = q\mathbf{v} \times \mathbf{B} \ . \tag{2.6}$$

The solution describes particle circular motion around a point, called the *guiding center*, in the plane perpendicular to the magnetic field. The frequency of gyration is

$$\omega_c = \frac{|q|\,B}{m} \ , \tag{2.7}$$

referred to as the *cyclotron frequency* or the *Larmor frequency* [5], here $B = |\mathbf{B}|$ is the magnitude of the magnetic field. The direction of the circular motion depends on the sign of the particle charge such that the generated magnetic field will decrease the total magnetic field. The guiding center also moves along the magnetic field with a speed $v_\parallel$, so the resulting motion is helical.

2.1.2 Particle Drifts

In the presence of a force or when the fields are slowly varying in space the resulting motion is a drift of the particles across the magnetic field lines. If the fields are inhomogeneous, we can no longer solve the equation of motion exactly. When they are slowly varying however, we can use a perturbative approach. By slowly we mean that $r_L \ll L$ is satisfied, where r_L is the radius

of the gyration around the guiding center, called the *Larmor radius*, and L is the length scale characterizing the variation of the fields. We then write

$$\mathbf{v} = \mathbf{v}_{gc} + \mathbf{v}_L \tag{2.8}$$

where $\mathbf{v}_{gc}$ is the guiding center velocity and $\mathbf{v}_L$ is the velocity of the Larmor gyration. We can express the guiding center velocity as

$$\mathbf{v}_{gc} = \mathbf{v}_d + \mathbf{v}_\parallel \ , \tag{2.9}$$

where $\mathbf{v}_d$ and $\mathbf{v}_\parallel$ are the drift- and parallel velocity, respectively. The parallel motion is determined by

$$m\frac{dv_\parallel}{dt} = qE_\parallel - \mu\nabla_\parallel B \ , \tag{2.10}$$

where

$$\nabla_\parallel = \mathbf{b}\cdot\nabla \ , \quad \mathbf{b} \equiv \mathbf{B}/B \tag{2.11}$$

is the gradient along the magnetic field, and

$$\mu = \frac{mv_L^2}{2B} \tag{2.12}$$

is the magnetic moment of the gyrating particle.

The perpendicular motion of the guiding center motion is a drift across the magnetic field lines, and can be expressed as [6]

$$\mathbf{v}_d = \frac{\mathbf{E}\times\mathbf{B}}{B^2} + \frac{v_L^2}{2\omega_c}\mathbf{b}\times\nabla\ln B + \frac{v_\parallel^2}{\omega_c}\times\vec{\kappa} \ , \tag{2.13}$$

where

$$\vec{\kappa} \equiv (\mathbf{b}\cdot\nabla)\mathbf{b} \ , \tag{2.14}$$

is the magnetic field curvature. The different terms in the drift velocity (2.13) are called the $\mathbf{E}\times\mathbf{B}$-, the ∇B- and the curvature drift respectively. Note that, the drift velocity is only valid for weakly varying electric fields when the orbit nearly closes in on itself after one Larmor gyration.

Let us consider now an equilibrium plasma with no equilibrium electric field and under the assumption of

$$\beta \equiv \frac{P}{B^2/2\mu_0} \ll 1 \ , \tag{2.15}$$

where P is the particle pressure. Thus, β is the ratio of particle and magnetic pressures which is assumed to be low, called the low β limit. In this limit the magnetic curvature becomes

$$\vec{\kappa} \approx \frac{\nabla_\perp B}{B} = \frac{\mathbf{b}\times(\nabla B\times\mathbf{b})}{B} \ , \tag{2.16}$$

and the guiding center velocity (2.9) can be written as

$$\mathbf{v}_{gc} \approx v_{\parallel}\mathbf{b} + \frac{1}{\omega_c B}\left[v_{\parallel}^2 + \frac{1}{2}v_L^2\right]\mathbf{b}\times\nabla B \ . \tag{2.17}$$

2.1.3 Adiabatic Invariants

For a Hamiltonian system that consists of rapid oscillations superimposed on a slow drift, there always exist adiabatic invariants [6]. This is also the case of a charged particle in a strong magnetic field where the rapid oscillation is the Larmor gyration. When the magnetic field changes slowly in space and time the magnetic moment (2.12) is a constant of motion, called the *first adiabatic invariant*.

Assume that the magnetic field changes sufficiently slow for the Larmor radius of a particle to be approximately constant during each orbit. If we dot the Lorentz force equation (2.5) with the velocity $\mathbf{v}$, and neglect the drift of the particle in the LHS, the result is

$$\frac{d}{dt}\left(\frac{mv_{\parallel}^2}{2} + \frac{mv_L^2}{2}\right) = qv_{\parallel}E_{\parallel} + q\mathbf{v}_{\perp}\cdot\mathbf{E} \ , \tag{2.18}$$

which together with equation (2.10) becomes

$$\frac{d}{dt}\left(\frac{mv_L}{2}\right) = \mu v_{\parallel}\nabla_{\parallel}B + q\mathbf{v}_{\perp}\cdot\mathbf{E} \ . \tag{2.19}$$

We average over a Larmor orbit

$$\langle\mathbf{v}_{\perp}\cdot\mathbf{E}\rangle_L = \frac{\omega_c}{2\pi}\oint_{orbit}\mathbf{E}\cdot\mathbf{v}_{\perp}\,\mathrm{d}t \ . \tag{2.20}$$

Integration of the Maxwell equation (2.4a) over the gyration surface, and using Stoke's theorem, then results in

$$\oint\mathbf{E}\cdot\,\mathrm{d}\mathbf{l} = \frac{\omega_c r_L^2}{2}\frac{\partial B}{\partial t} \ , \tag{2.21}$$

where $r_L = v_L/\omega_c$ is the Larmor radius. When using (2.21) and $\mathbf{v}_{\perp}\mathrm{d}t = \mathrm{d}\mathbf{l}$, equation (2.20) becomes

$$\langle\mathbf{v}_{\perp}\cdot\mathbf{E}\rangle_L = \frac{\omega_c r_L^2}{2}\frac{\partial B}{\partial t} \ . \tag{2.22}$$

Finally, using (2.7), the Larmor average of (2.19) becomes

$$\left\langle\frac{d}{dt}\left(\frac{mv_L^2}{2}\right)\right\rangle_L = \frac{mv_L^2}{2B}\frac{dB}{dt} \ , \tag{2.23}$$

where $\frac{dB}{dt} = \frac{\partial B}{\partial t} + v_\parallel \nabla_\parallel B$. The Larmor orbit kinetic energy can be expressed as $W_\perp = mv_L^2/2$, equation (2.23) then becomes

$$\frac{1}{W_\perp}\frac{dW_\perp}{dt} = \frac{1}{B}\frac{dB}{dt} \tag{2.24}$$

which has the solution

$$\frac{W_\perp}{B} \equiv \mu = Const. \tag{2.25}$$

Furthermore, in the absence of forces, the particle kinetic energy

$$W = \frac{mv^2}{2} \ , \tag{2.26}$$

is an exact constant of motion. Together with the magnetic moment we then write the expression for the parallel particle velocity in terms of the invariants of the particle motion,

$$v_\parallel = \pm\sqrt{\frac{2}{m}(W - \mu B)} \ , \tag{2.27}$$

which changes only due to the variation of B. The guiding center velocity (2.17) can then be expressed as [7]

$$\mathbf{v}_{gc} = v_\parallel \mathbf{b} - v_\parallel \mathbf{b} \times \nabla \left(\frac{v_\parallel}{\omega_c}\right) \ . \tag{2.28}$$

There are also higher order adiabatic invariants associated with other periodic motions. For instance, when considering timescales longer than the bounce period of a so called trapped particle that reverses it's motion parallel to the magnetic field, there is a second order adiabatic invariant:

$$J = \oint v_\parallel \, \mathrm{dq} \ , \tag{2.29}$$

where q is the arc length along the bounce orbit.

2.2 Kinetic Theory

The most accurate closure of Maxwell's equations is the kinetic model, where the particle distribution functions, $f_e(\mathbf{r}, \mathbf{v}; t)$ and $f_i(\mathbf{r}, \mathbf{v}; t)$ for electrons and ions, respectively, provide a statistical description of the system. Then, the kinetic equations governing the evolution of the distribution functions in the six-dimensional phase space need to be solved, which is in general complicated. The evolution equation is the *Boltzmann equation*

$$\frac{\partial f}{\partial t} + \mathbf{v} \cdot \frac{\partial f}{\partial \mathbf{r}} + \frac{q}{m}(\mathbf{E} + \mathbf{v} \times \mathbf{B}) \cdot \frac{\partial f}{\partial \mathbf{v}} = \left(\frac{\partial f}{\partial t}\right)_c , \tag{2.30}$$

where $(\partial f/\partial t)_c$ is the collision operator representing the rate of change of f due to collisions. Note that there is no exact expression for the collision operator. In general it is a complicated nonlinear function of f. Collisions can however be neglected when $\nu_c \ll \omega$, where ν_c is the collision frequency and ω is the frequency characterizing the time rate of change of the macroscopic forces. The Boltzmann equation (2.30) then becomes

$$\frac{\partial f}{\partial t} + \mathbf{v} \cdot \frac{\partial f}{\partial \mathbf{r}} + \frac{q}{m}(\mathbf{E} + \mathbf{v} \times \mathbf{B}) \cdot \frac{\partial f}{\partial \mathbf{v}} = 0 , \tag{2.31}$$

which is the so called *Vlasov equation*.

For a steady state, homogeneous and collisionless plasma, the solution to (2.30) is the Maxwell distribution function [5]

$$f = n \left(\frac{m}{2\pi k_B T}\right)^{\frac{3}{2}} e^{\frac{-mv^2}{2k_B T}} . \tag{2.32}$$

In the kinetic model, we can use velocity moments to express the quantities in Maxwell's equations, such as

$$\rho = q \int f \, \mathrm{d}\mathbf{v} , \tag{2.33a}$$

$$\mathbf{J} = q \int \mathbf{v} f \, \mathrm{d}\mathbf{v} . \tag{2.33b}$$

2.3 Magnetohydrodynamic Model

In fluid models, we use macroscopic properties such as densities, temperatures and pressures to describe the plasma. These quantities are derived from the velocity moments of the distribution function for each plasma species. When using the moment procedure, it always leads to a system of more unknowns than equations so one needs to truncate the series of moments by some proper assumptions, usually referred to as closure.

Magnetohydrodynamics (MHD), which is often used to study macroscopic plasma phenomena, is derived by taking the fluid models one step further: Here, ion and electron fluids are combined into one single fluid. For the MHD description to be valid the plasma needs to be collision dominated, which requires a locally Maxwellian distribution function. This also means that the MHD time scale must be sufficiently long for there to be adequately many collisions. The displacement current can then be neglected in the Maxwell

equations. Without the displacement term, Ampére's law (2.4b) is not Lorentz invariant, which means that it is only valid for velocities much lower than the speed of light in vacuum. This is not a problem in the MHD description, since the time scale is much longer than the time it takes light to traverse the plasma. Furthermore, the dominant fluid velocity is the $\mathbf{E} \times \mathbf{B}$-drift, which means that MHD describes low frequency phenomena with respect to the plasma frequency (2.2)

$$\omega \ll \omega_p \ . \tag{2.34}$$

Finally, the plasma pressure is assumed to be finite compared to the magnetic pressure.

The characteristic properties of the MHD fluid are expressed by the total mass density

$$\rho_m \equiv m_i n_i + m_e n_e \ , \tag{2.35}$$

where m_i, m_e and n_i, n_e are the masses and number densities of ions and electrons, the total charge density

$$\rho \equiv e(Z_i n_i - n_e) \ , \tag{2.36}$$

the center-of-mass velocity

$$\mathbf{v} \equiv \frac{m_i n_i \mathbf{u}_i + m_e n_e \mathbf{u}_e}{m_i n_i + m_e n_e} \ , \tag{2.37}$$

where $\mathbf{v}_i$ and $\mathbf{v}_e$ are the fluid velocity vectors of ions and electrons, and the current density

$$\mathbf{J} \equiv e(Z_i n_i \mathbf{u}_i - n_e \mathbf{u}_e) \ , \tag{2.38}$$

where Z_i is the ion charge number. With the assumption of quasi-neutrality, $Z_i n_i \approx n_e$, one finds $\rho = 0$ and $\mathbf{v} \approx \mathbf{v}_i$. Under the further assumption that the total pressure is $P = P_e + P_i$, where P_e and P_i are the scalar electron and ion pressures, the MHD set of equations becomes

- The continuity equation

$$\frac{\partial \rho_m}{\partial t} + \nabla \left(\rho_m \mathbf{v} \right) = 0 \ , \tag{2.39a}$$

- The momentum equation

$$\rho_m \frac{d\mathbf{v}}{dt} = \mathbf{J} \times \mathbf{B} - \nabla P \ , \tag{2.39b}$$

- The adiabatic equation of state

$$\frac{d}{dt}\left(\frac{P}{\rho_m^\gamma}\right) = 0 \ , \tag{2.39c}$$

- The resistive Ohm law

$$\mathbf{E} + \mathbf{v} \times \mathbf{B} = \eta \mathbf{J} \ , \tag{2.39d}$$

- The Ampére law (without the displacement current)

$$\nabla \times \mathbf{B} = \mu_0 \mathbf{J} \ , \tag{2.39e}$$

- The Faraday law

$$\nabla \times \mathbf{E} = -\frac{\partial \mathbf{B}}{\partial t} \ . \tag{2.39f}$$

Here, γ is the ratio of specific heats at constant pressure and constant volume and η is the plasma resistivity. Note that the Maxwell relation $\nabla \cdot \mathbf{B} = 0$ is implied. The fact that the displacement current is neglected in Ampére's law also means that

$$\nabla \cdot \mathbf{J} = 0 \ . \tag{2.40}$$

In many cases a further simplification is made by assuming that the plasma conductivity is so high that $\eta = 0$. Then, the so called ideal Ohm law reads

$$\mathbf{E} + \mathbf{v} \times \mathbf{B} = 0 \ . \tag{2.41}$$

The resulting model is called ideal MHD, and is used to describe plasma equilibrium and stability of waves in the low frequency range, $\omega \ll \omega_p$. It seems to provide an accurate description of the macroscopic fusion plasma behaviour even though it is not obvious that the criteria for ideal MHD are fulfilled [8]. For instance, one of the consequences of ideal Ohm's law is that the parallel component of the electric field is zero.

2.3.1 Equilibrium Analysis

In equilibrium the momentum equation (2.39b) describes a force balance

$$\mathbf{J}_0 \times \mathbf{B}_0 = \nabla P_0 \ , \tag{2.42}$$

where the subscript 0 denotes equilibrium quantities. This means that the plasma can be confined by a magnetic field if the plasma pressure is balanced by a magnetic pressure. An important result from the force balance equation (2.42) together with Ampére's law (2.39e) is that the sum of the particle

pressure, P_0, and magnetic pressure is constant when the magnetic field is homogeneous in the direction of the field. One can show this by substituting the current in Ampére's law into the force balance equation with the result

$$\nabla P_0 = \frac{1}{\mu_0}(\nabla \times \mathbf{B}_0) \times \mathbf{B}_0 = \frac{1}{\mu_0}\left[(\mathbf{B}_0 \cdot \nabla)\mathbf{B}_0 - \frac{\nabla B_0^2}{2}\right] . \tag{2.43}$$

When $\mathbf{B}_0 \cdot \nabla = 0$ equation (2.43) implies

$$P_0 + \frac{B_0^2}{2\mu_0} = Const. \tag{2.44}$$

Note that if the equilibrium plasma is uniform,

$$\nabla \times \mathbf{B}_0 = 0 , \tag{2.45}$$

Ampére's law (2.39e) becomes $\mathbf{J}_0 = 0$ which together with the force balance (2.42) results in a constant equilibrium pressure P_0.

2.3.2 Stability Analysis

When we have an equilibrium plasma the next step is to look at its stability properties. To simplify the analysis we will restrict ourselves to linear stability, and represent the dependent variables as the sum of an equilibrium part plus a small perturbation,

$$\mathbf{B} = \mathbf{B}_0 + \mathbf{B}_1 , \quad \mathbf{J} = \mathbf{J}_0 + \mathbf{J}_1 , \tag{2.46a}$$

$$P = P_0 + P_1 , \quad \rho = \rho_0 + \rho_1 , \tag{2.46b}$$

where the equilibrium and perturbed quantities are denoted by the subscripts 0 and 1, respectively. We can transform the MHD equations to a frame of reference moving with the equilibrium velocity $\mathbf{v}_0$, which means that $\mathbf{v} = \mathbf{v}_1$ and, by the ideal Ohm law (2.41), $\mathbf{E} = \mathbf{E}_1$. The equilibrium quantities are then functions of space only while the perturbations are of space and time. From the set of equations (2.39a) - (2.39f), with the ideal Ohm law, we obtain sets of equations to zeroth order for the equilibrium (cf. section 2.3.1) and to first order for the stability:

- Equilibrium

$$\mathbf{J}_0 \times \mathbf{B}_0 = \nabla P_0 , \tag{2.47a}$$

$$\nabla \times \mathbf{B}_0 = \mu_0 \mathbf{J}_0 , \tag{2.47b}$$

- Linear stability

$$\frac{\partial \rho_1}{\partial t} + \nabla \cdot (\rho_0 \mathbf{v}_1) = 0 \ , \tag{2.47c}$$

$$\rho_0 \frac{\partial \mathbf{v}_1}{\partial t} = \mathbf{J}_0 \times \mathbf{B}_1 + \mathbf{J}_1 \times \mathbf{B}_0 - \nabla P_1 \ , \tag{2.47d}$$

$$\frac{\partial P_1}{\partial t} + \mathbf{v}_1 \cdot \nabla P_0 + \frac{\gamma P_0}{\rho_0} \left(\frac{\partial \rho_1}{\partial t} + \mathbf{v}_1 \cdot \nabla \rho_0 \right) = 0 \ , \tag{2.47e}$$

$$\frac{\partial \mathbf{B}_1}{\partial t} = \nabla \times (\mathbf{v}_1 \times \mathbf{B}_0) \ , \tag{2.47f}$$

$$\nabla \times \mathbf{B}_1 = \mu_0 \mathbf{J}_1 \ . \tag{2.47g}$$

Since the equilibrium equations are independent of time,

$$Q_0(\mathbf{r}, t) = Q_0(\mathbf{r}) \ , \tag{2.48a}$$

and the stability equations are linear, we can represent the perturbations as normal modes

$$Q_1(\mathbf{r}, t) = Q_1(\mathbf{r}) e^{-i\omega t} \ . \tag{2.48b}$$

If we introduce the perturbed displacement vector $\vec{\xi}$ as

$$\mathbf{v}_1 = \frac{\partial \vec{\xi}}{\partial t} = -i\omega \vec{\xi}(\mathbf{r}) e^{-i\omega t} \ , \tag{2.49}$$

the linear stability equations (2.47c) yield [8]

$$-\omega^2 \rho_1 \vec{\xi} = \mathbf{F}(\vec{\xi}) \ , \tag{2.50}$$

which is an eigenvalue equation with the frequency ω as the eigenvalue. Here, $\mathbf{F}$ is given by

$$\begin{aligned} \mathbf{F}(\vec{\xi}) = \frac{1}{\mu_0} \Big\{ (\nabla \times \mathbf{B}_0) \times \left[\nabla \times (\vec{\xi} \times \mathbf{B}_0) \right] + \nabla \times \left[\nabla \times (\vec{\xi} \times \mathbf{B}_0) \right] \times \mathbf{B}_0 \Big\} \\ + \nabla (\vec{\xi} \cdot \nabla P_0 + \gamma P_0 \nabla \cdot \vec{\xi}) \ . \end{aligned} \tag{2.51}$$

What is important to note is that $\mathbf{F}$ is Hermitian [8]. This means that $\omega^2 \in \mathfrak{R}$. If $\omega^2 > 0$ then $\omega \in \mathfrak{R}$ and the solution to (2.50) is a mode with frequency ω, and if $\omega^2 < 0$ then $i\omega \equiv \gamma \in \mathfrak{R}$ and there is an instability with $Re(\omega) = 0$. The eigenvalue problem (2.50) needs to be solved for a given magnetic field in a certain geometry, with given initial values and boundary conditions. Note that, it is customary to Fourier transform.

The simplest case of a homogeneous magnetic field in an infinite geometry results in two kinds of waves, the shear and compressional Alfvén waves. For us the most interesting is the shear Alfvén wave

$$\omega^2 = k_\parallel^2 v_A^2 \ , \tag{2.52}$$

where $k_\parallel$ is the parallel wave number with respect to the magnetic field and v_A is the *Alfvén velocity*

$$v_A^2 \equiv \frac{B^2}{\mu_0 \rho_0} \ . \tag{2.53}$$

This wave propagates along and at angles to the magnetic background field but all fluctuations are perpendicular to the magnetic field, hence the name shear wave. Furthermore, this wave is incompressional and therefore has no density or pressure fluctuations.

For later purposes, we consider a nonuniform magnetic field in a general geometry: The linearization procedure leads to the following equation [9]:

$$\nabla \cdot \left(\frac{\omega^2}{v_A^2} \nabla_\perp \phi \right) + \mathbf{B}_0 \cdot \nabla \left\{ \frac{1}{B_0^2} \nabla \cdot \left[B_0^2 \nabla_\perp \left(\frac{\mathbf{B}_0 \cdot \nabla \phi}{B_0^2} \right) \right] \right\} = 0 \ , \tag{2.54}$$

for the electrostatic potential ϕ of a shear Alfvén wave with high toroidal mode number and in the low β limit.

3

Toroidal Systems

Magnetic confinement of plasma particles can be implemented in several different ways. Many of these methods utilize externally generated magnetic fields designed in such a way that the field lines define a torus, i.e a cylinder deformed until it closes on itself [8]. The most common type of toroidal magnetic confinement device is the so called *tokamak*. In tokamaks, the plasma particles are confined by means of a large magnetic field in the toroidal direction, which is generated by external coils. This results in circulating particles, which follow the magnetic field lines around the torus. However, a small poloidal field component produced by a transformer induced plasma current is also necessary in order to average out radial drifts. This is because the toroidal magnetic field varies radially in space, with the associated ∇B- and curvature drifts of the particles resulting in a vertical separation of electrons and ions. The charge separation leads in turn to a potential difference and an associated $\mathbf{E} \times \mathbf{B}$-drift, which results in a radial drift outwards of both ions and electrons.

In general, a tokamak cross section may be elliptically elongated, D-shaped and asymmetric with respect to the horizontal and vertical midplanes. In this thesis, however, we will use a circular approximation described by the toroidal coordinates (r, θ, ζ) and (R, ζ, z), see Figure(3.1). The asymmetry with respect to the vertical midplane will be included in some calculations as a so called Shafranov shift.

3.1 Equilibrium Analysis

Tokamak equilibria are efficiently analyzed by the MHD equilibrium equations (2.47a) and (2.47b). Note that this implies that

$$\mathbf{B}_0 \cdot \nabla P_0 = 0 \ , \tag{3.1}$$

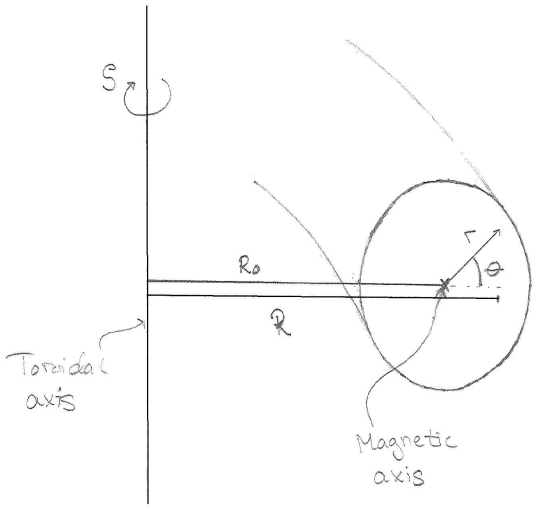

Figure 3.1: Poloidal cross section of a circular tokamak, displaying the toroidal coordinates (r, θ, ζ).

which means that the magnetic field lines lie on surfaces of constant pressure. Since the magnetic field has both poloidal and toroidal components, these so called flux surfaces close on themselves both toroidally and poloidally, and must therefore be nested tubes with the innermost known as the magnetic axis. Hence, $P = P(\psi)$, where ψ, the poloidal flux, is constant along magnetic field lines, i.e a function only of r. In a toroidal device the poloidal magnetic flux can be expressed as

$$\psi = \int_{V(r)} \mathbf{B}_0 \cdot \nabla\theta \, \mathrm{d}^3x \ , \tag{3.2}$$

where $\mathrm{d}^3x = \sqrt{g}\mathrm{d}r\mathrm{d}\theta\mathrm{d}\zeta$, $1/\sqrt{g}$ is the Jacobian and $V(r)$ is the volume bounded by the magnetic flux surface of radius r.

In a tokamak, we may express the magnetic field as

$$\mathbf{B} = \mathbf{B}_P + \mathbf{B}_T \ , \tag{3.3}$$

where $B_T \gg B_P$ and the toroidal magnetic field strength varies radially as R^{-1}:

$$B_T \equiv \frac{I(r)}{R} = \frac{B_s(r)}{1 + \epsilon\cos\theta} \ . \tag{3.4}$$

Here, $B_s \equiv I(r)/R_0$, $I(r)$ is the current in the exterior field coils, R_0 is the distance from the axis of symmetry to the magnetic axis and

$$\epsilon \equiv r/R_0 \tag{3.5}$$

is the inverse aspect ratio, which is generally small throughout a tokamak. Another useful way to express the magnetic field is

$$\mathbf{B} = I(\psi)\nabla\zeta + \nabla\zeta \times \nabla\psi \ . \tag{3.6}$$

If we consider a plasma in an axisymmetric magnetic field, all derivatives with respect to the toroidal angle ζ vanish. Using the force balance equation (2.50), and the magnetic field (3.6) together with Ampére's law, we get the Grad-Shafranov equation [6]

$$R^2\nabla\cdot\left(\frac{\nabla\psi}{R^2}\right) = -\mu_0 R^2\frac{dP}{d\psi} - I(\psi)\frac{dI}{d\psi} \ , \tag{3.7}$$

whose solutions describe the possible plasma equilibria.

3.2 Guiding Center Motion

In the absence of wave fields, the trajectory of a particle can be characterized by the following three invariants of motion:

- The total particle energy, E
- The generalized toroidal momentum, p_ζ
- The magnetic moment, μ

To derive the invariants we use the Lagrangian for a single particle in an electromagnetic field

$$\mathcal{L} = \frac{Mv^2}{2} + Ze\left(\mathbf{v}\cdot\mathbf{A} - \phi\right) \ , \tag{3.8}$$

where M, Ze and $\mathbf{v}$ are the mass, charge and velocity of the particle and $\mathbf{A}$ is the vector potential used to describe the electric and magnetic field according to

$$\mathbf{E} = -\nabla\phi - \frac{\partial\mathbf{A}}{\partial t} \ , \tag{3.9}$$

$$\mathbf{B} = \nabla\times\mathbf{A} \ . \tag{3.10}$$

The total energy of the particle is given by $E = H$, where H is the Hamiltonian of the system and can be found by the Legandre transformation [10]

$$H = \mathbf{v}\cdot\frac{\partial\mathcal{L}}{\partial\mathbf{v}} - \mathcal{L} = W + Ze\phi \ , \tag{3.11}$$

where W is the particle kinetic energy. By the Euler-Lagrange equation

$$\frac{\partial \mathcal{L}}{\partial r^i} = \frac{d}{dt}\left(\frac{\partial \mathcal{L}}{\partial \dot{r}^i}\right) \ , \tag{3.12}$$

where r^i, $i = 1, 2, 3$, represent the coordinates (in this case (r, θ, ζ)), we find that

$$\frac{dE}{dt} = \frac{\partial H}{\partial t} = 0 \ . \tag{3.13}$$

Note that in the presence of a wave field, $\mathcal{L}$ will depend explicitly on time and E is no longer invariant.

From the Lagrangian description we also find the second invariant, the generalized momentum,

$$p_\zeta = \frac{\partial \mathcal{L}}{\partial \dot{\zeta}} \ . \tag{3.14}$$

By the Euler-Lagrange equation we see that whenever the Lagrangian does not depend on a certain variable, the associated canonical momentum is an invariant. Thus, for an axisymmetric tokamak, independent on the toroidal angle ζ,

$$\frac{dp_\zeta}{dt} = 0 \ . \tag{3.15}$$

The generalized momentum can be expressed, using equations (3.8) and (3.14), as

$$p_\zeta = MRv_\zeta + ZeA_\zeta \ . \tag{3.16}$$

where v_ζ and A_ζ are the toroidal components of $\mathbf{v}$ and $\mathbf{A}$. Note that, in the presence of an external wave field depending on ζ, axisymmetry will be broken and p_ζ will no longer be invariant.

Finally, the magnetic moment, given by (2.12), was shown in section (2.1.3) to be an adiabatic invariant, i.e constant as long as the gradients in the magnetic field are sufficiently small as compared to the plasma dimensions. This is also true in a tokamak since the magnetic field varies on a large scale as compared to the Larmor radius.

In the low β limit and in the absence of forces, the particle guiding center motion can be easily calculated using (2.28). Componentwise in the toroidal coordinates (r, θ, ζ), we have

$$\frac{dr}{dt} = \hat{r} \cdot \mathbf{v}_{gc} = \frac{v_\parallel}{r}\frac{\partial}{\partial \theta}\left(\frac{v_\parallel}{\omega_c}\right) \ , \tag{3.17a}$$

$$\frac{d\theta}{dt} = \frac{\hat{\theta}}{r} \cdot \mathbf{v}_{gc} = \frac{v_\parallel}{qR_0}\left[1 - \frac{q}{\epsilon}\frac{\partial}{\partial r}\left(\frac{v_\parallel}{\omega_c}\right)\right] \ , \tag{3.17b}$$

$$\frac{d\zeta}{dt} = \frac{\hat{\zeta}}{R} \cdot \mathbf{v}_{gc} = \frac{v_\parallel}{qR}\left[1 + \frac{\epsilon}{q}\frac{\partial}{\partial r}\left(\frac{v_\parallel}{\omega_c}\right)\right] \ , \tag{3.17c}$$

where q is the safety factor,

$$q = \frac{\nabla\zeta \cdot \mathbf{B}_0}{\nabla\theta \cdot \mathbf{B}_0} \ , \tag{3.18}$$

i.e the number of toroidal revolutions a field line executes during one poloidal revolution.

3.3 Trapped and Passing Particles

The magnetic field (3.4) has a maximum poloidally. Due to the conservation of the magnetic moment μ, this means that particles may bounce when approaching this maximum, depending on their ratio of perpendicular and parallel energy. Hence, there are two kinds of particles, trapped and passing particles. The trapped particles bounce toroidally and poloidally at the points where their velocities parallel to the total magnetic field vanish, while the passing particles encircle the magnetic axis and the torus toroidally and poloidally.

Following [7] we insert the expression (3.4) for the magnetic field into the expression (2.27) for the parallel velocity, we obtain

$$v_\parallel = \frac{v_{\parallel 0}}{\kappa}\sqrt{\kappa^2 - \sin^2\frac{\theta}{2}} \ , \tag{3.19}$$

where we have defined the trapping parameter

$$\kappa^2 \equiv \frac{W - \mu B_s(1-\epsilon)}{2\mu B_s \epsilon} \ , \tag{3.20}$$

and

$$v_{\parallel 0} = v_\parallel(\theta = 0) = \pm\kappa\sqrt{\frac{\mu B_s \epsilon}{M}} \ , \tag{3.21}$$

Note that W and μ are invariants of the particle motion, and that we have assumed that $B_s(r)$ is constant. Hence, κ^2 depends on the radius r only through the ϵ-factor. The trapped particles reverse their motion parallel to the magnetic field at the poloidal angles $\theta_B = \pm 2\arcsin\kappa$ where $v_\parallel = 0$. By conservation of energy and magnetic moment, we see that $\kappa^2 < 1$ for trapped particles, and that the passing particles satisfy $\kappa^2 > 1$. Due to the curvature and ∇B-drifts, the particle orbits may also differ slightly radially from the magnetic flux surfaces. This is known as finite orbit width effects, and is the result of the second terms within the brackets on the right hand sides of (3.17b) and (3.17c).

The period of a poloidal orbit for trapped and passing particles is

$$\tau_B = \int_0^{\tau_B} dt \ . \tag{3.22}$$

To calculate it we use the expression for the θ-component of the guiding center motion (3.17b) to relate t and θ

$$dt = \frac{qR_0}{v_\parallel}\left[1 - \frac{q}{\epsilon}\frac{\partial}{\partial r}\left(\frac{v_\parallel}{\omega_c}\right)\right]^{-1} d\theta \ . \tag{3.23}$$

Note that all quantities in (3.23) are to be evaluated at the average particle radial position during a poloidal orbit. When we neglect the finite orbit width effect we then have

$$dt \approx \frac{qR_0}{v_\parallel} d\theta \ , \tag{3.24}$$

and the period of a poloidal orbit for passing particles becomes

$$\begin{aligned}\tau_B = \int_0^{\tau_B} dt \approx \frac{qR_0\kappa}{v_{\parallel 0}} \int_{\theta(0)}^{\theta(\tau_B)} \frac{d\theta}{\sqrt{\kappa^2 - \sin^2\frac{\theta}{2}}} = \\ = \frac{4qR_0}{v_{\parallel 0}} \int_0^{\frac{\pi}{2}} \frac{d\phi}{\sqrt{1 - \kappa^{-2}\sin^2\phi}} = \frac{4qR_0}{v_{\parallel 0}} K\left(\kappa^{-1}\right) \ ,\end{aligned} \tag{3.25}$$

where $K(\kappa)$ is the complete elliptic integral of the first kind. The poloidal frequency is then

$$\omega_B = \frac{2\pi}{\tau_B} = \frac{\pi v_{\parallel 0}}{2qR_0 K(\kappa^{-1})} \ . \tag{3.26}$$

For the trapped particles, the bounce period between the angles $\theta_B = \pm 2\arcsin\kappa$ is

$$\begin{aligned}\tau_B = 2\frac{qR_0\kappa}{v_{\parallel 0}} \int_{-\theta_B}^{\theta_B} \frac{d\theta}{\sqrt{\kappa^2 - \sin^2\frac{\theta}{2}}} = 8\frac{qR_0\kappa}{v_{\parallel 0}} \int_0^{\arcsin\kappa} \frac{d\phi}{\sqrt{\kappa^2 - \sin^2\phi}} = \\ = \{\sin\phi = \kappa\sin\varphi\} = \frac{8qR_0\kappa}{v_{\parallel 0}} \int_0^{\frac{\pi}{2}} \frac{d\varphi}{\sqrt{1 - \kappa^2\sin^2\varphi}} = \frac{8qR_0\kappa}{v_{\parallel 0}} K\left(\kappa\right) \ ,\end{aligned} \tag{3.27}$$

and the associated frequency becomes

$$\omega_B = \frac{2\pi}{\tau_B} = \frac{\pi v_{\parallel 0}}{4qR_0\kappa K\left(\kappa\right)} \ . \tag{3.28}$$

3.4 Toroidal Instabilities

In periodic, toroidal systems, any linear instability may be Fourier decomposed according to

$$\phi(r,\theta,\zeta;t) = \sum_{m,n} \phi_{m,n}(r) e^{i(n\zeta - m\theta - \omega t)} \ , \tag{3.29}$$

where m and n are the so called poloidal and toroidal mode numbers. If the inverse aspect ratio ϵ is small, as in tokamaks, the equilibrium magnetic field is dominated by the toroidal magnetic field (3.4). This magnetic field is symmetric in ζ, but because of the $\epsilon \cos\theta$ term there is no symmetry in θ. For Alfvén type instabilities this leads to a coupling between neighboring poloidal harmonics of ϕ. If we assume that the mode numbers m and n are large, the equations describing this coupling are [11]

$$\begin{bmatrix} \mathfrak{L}_m & \mathfrak{L}_1 \\ \mathfrak{L}_1 & \mathfrak{L}_{m+1} \end{bmatrix} \begin{bmatrix} \phi_m \\ \phi_{m+1} \end{bmatrix} = 0 \ , \tag{3.30}$$

where

$$\mathfrak{L}_m = \frac{d}{dr}\left[\left(\omega^2 - \omega_A^2\right)\frac{d}{dr}\right] - \frac{m^2}{r^2}\left(\omega^2 - \omega_A^2\right) \ , \tag{3.31a}$$

$$\mathfrak{L}_1 = \hat{\epsilon}\,\omega^2 \frac{d^2}{dr^2} \ . \tag{3.31b}$$

Here, the Alfvén frequency is defined as

$$\omega_A(r) \equiv k_{\parallel m n}(r)\, v_A(r) \ , \tag{3.32}$$

and the parallel wave number and the Alfvén velocity are given by

$$k_{\parallel m n} \equiv \mathbf{b}\cdot\mathbf{k} = \frac{1}{qR_0}(nq - m) \ , \tag{3.33}$$

$$v_A^2(r) = \frac{B(r)^2}{\mu_0 \rho(r)} \ , \tag{3.34}$$

with $\hat{\epsilon} = 5r/2R_0$ [12]. Note that the Alfvén frequency ω_A varies radially via the combinded variation of $k_{\parallel m n}$ and v_A.

3.4.1 Cylindrical Limit

In the cylindrical limit $\epsilon \to 0$, the magnetic field strength (3.4) is approximately constant. This means that the translational symmetry in θ is restored, and the set of coupled equations (3.30) decouples into

$$\frac{d}{dr}\left[(\omega^2 - \omega_A^2)\frac{d\phi_m}{dr}\right] - \frac{m^2}{r^2}(\omega^2 - \omega_A^2)\phi_m = 0 \ , \tag{3.35}$$

for each poloidal harmonic. A branch of solutions to (3.35) has $\omega^2 = \omega_A^2$. However, these modes are logaritmically divergent, as can be seen by Taylor expanding $\omega^2 - \omega_A^2$, and are therefore almost completely damped throughout the plasma. This damping is known as *continuum damping*, and the logaritmically divergent modes define the so called cylindrical Alfvén continuum. In Figure (3.2), the qualitative behaviour of the Alfvén frequency as a function of radius is plotted.

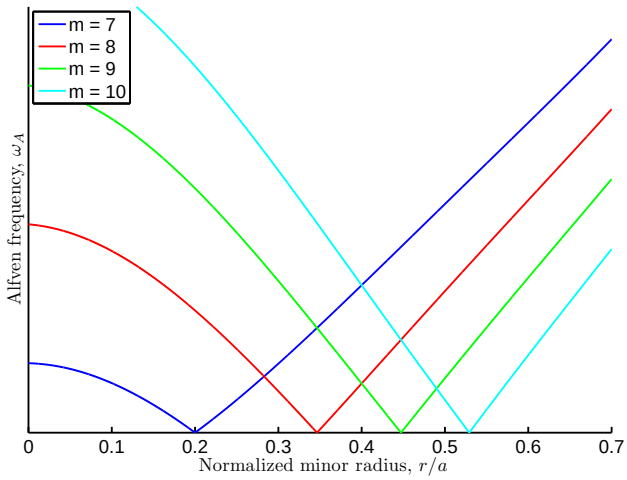

Figure 3.2: Qualitative figure displaying the Alfvén frequency ω_A when $n = 5$, using realistic profiles for the density, safety factor and magnetic field strength.

3.4.2 Toroidal Alfvén Eigenmodes

Toroidal Alfvén eigenmodes (TAEs) are discrete frequency waves [13] that exist due to toroidicity induced coupling between poloidal harmonics. In the cylindrical limit, neighbouring poloidal continua cross at the surfaces $r = r_m$ (see Figure (3.2)), where

$$k_{\parallel\, m\, n} v_A = -k_{\parallel\, m+1\, n} v_A \equiv \omega_0 \ , \tag{3.36}$$

which implies that

$$q\left(r_m\right) \equiv q_m = \frac{2m+1}{2n} \ . \tag{3.37}$$

Inserting (3.37) in (3.36) yields

$$\omega_0 = \frac{v_A}{2 q_m R_0} \ . \tag{3.38}$$

Accounting for toroidicity by letting ϵ become finite, only the proximity of r_m is affected, where small gaps of width $\Delta\omega \approx \hat{\epsilon}\,\omega_0$ are induced in the Alfvén continuum, see Figure (3.3). The distance between neighbouring such gaps is approximately [14]

$$|r_{m+1} - r_m| \approx \frac{r_m}{nqS} \ , \tag{3.39}$$

where the magnetic shear, S, is defined as

$$S \equiv \frac{r}{q}\frac{dq}{dr} \ . \tag{3.40}$$

Nonzero ϵ also results in a discrete frequency eigenmode, which forms due

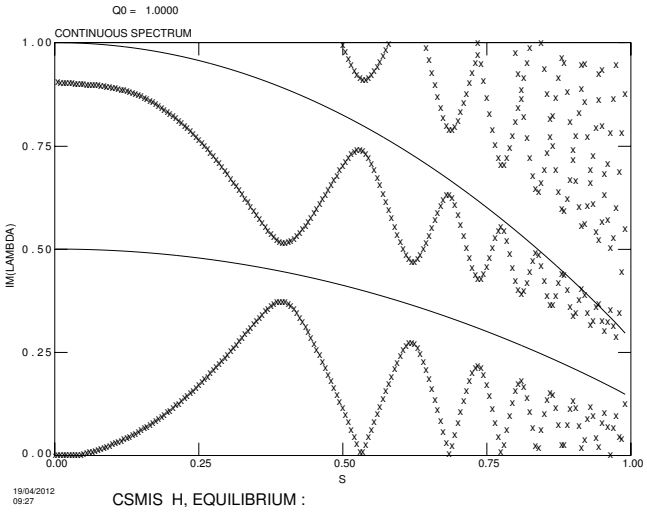

Figure 3.3: Alfvén continuum for $n = 4$, discharge 42979 at JET, as calculated by the MHD linear instability code CASTOR.

to the interaction of neighbouring poloidal harmonics in the vicinity of the gap. In the low shear limit, $S \ll 1$, the distance between the gaps (cf. Figure (3.39)) is sufficiently large for the eigenmode to be localized near its own gap and not interact with modes from neighbouring gaps. According to the boundary layer theory [14] which is used to analyze the system (3.30), the coupling between different harmonics takes place in a narrow inner region and in the outer region each poloidal mode satisfies the cylindrical mode equation (3.35). To determine the mode structure, a matching procedure for the outer and inner regions has to be used [14]. The result in the low shear limit is a discrete frequency eigenmode at the bottom of each toroidicity induced gap. The frequency of this downshifted eigenmode is given by

$$\omega_{TAE} = \omega_0 \left[1 - \hat{\epsilon}\left(1 - \frac{\pi^2 S^2}{8}\right)\right] \ . \tag{3.41}$$

Since the mode is inside the gap it does not fulfill the condition for continuum damping. This eigenmode is therefore weakly damped and it consists of an even combination of the coupled neighbouring poloidal harmonics, see Figure (3.4).

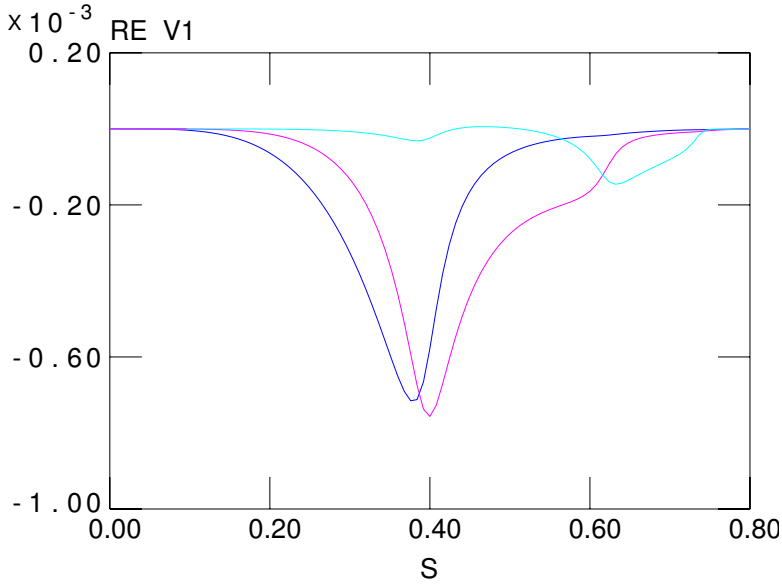

Figure 3.4: Coupled, neighbouring poloidal harmonics constituting an even TAE for $n = 4$, discharge 42979 at JET. The eigenmode is found by means of the MHD code MISHKA.

Note that to arrive at the system (3.30), ideal Ohm's law has been used, which neglects any parallel electric field. In the inner regions, we should really include both the toroidicity induced coupling and nonideal effects. The nonideal effects are due to parallel electron dynamics and first order finite ion Larmor radius (FLR) effects. Also note that the theory presented here only gives criteria for the existance of toroidal Alfvén eigenmodes. A driving mechanism is needed to excite these modes, such as e.g. resonant interaction between the wave and fast particles.

3.5 Excitation of Alfvénic Modes

The dispersion relation (2.50) has been derived within the framework of ideal MHD, using a linear approach where all quantities are assumed to consist of a stationary part and a small perturbation. This results in a real frequency $\omega = \omega_{TAE}$. Fast ions, with $v_f \gg v_{th}$, where v_{th} is the thermal velocity of the bulk ions in the plasma, need to be treated using kinetic theory. The result can then be added to the MHD result, with the fast particles contributing to

the imaginary part of the linear frequency, which becomes $\omega = \omega_{TAE} + i\gamma_L$ [15]. Since all perturbed quantities vary in time as $e^{-i\omega t}$, the fast particles result in an exponential growth of the wave provided that $\gamma_L > 0$. This also means that the linear theory is only valid initially.

Free energy is available to drive the mode when the fast particle pressure is large enough to overcome the total damping by the bulk plasma. For a TAE mode this is when [16, 17]

$$\frac{\gamma_L}{\omega_{TAE}} = -\left(1 - \frac{\omega_{*f}}{\omega_{TAE}}\right) F\left(\frac{v_f}{v_A}\right) \geq \frac{\gamma_d}{\omega_{TAE}} \ , \tag{3.42}$$

where ω_{TAE} is the frequency of the considered mode, γ_L is the linear growth rate of the wave caused by the fast particles, ω_{*f} is the fast particle drift frequency and γ_d is the total damping rate associated with the bulk plasma. The function $F\left(v_f/v_A\right)$ depends on the distribution function of the fast particles in velocity space.

In a tokamak, the fast ions gyrate in circles of radius $r_L \simeq v_f/\omega_{cf}$. Simultaneously, the density profile of the fast particles in a tokamak plasma decreases with increasing radius which means that there are more particles that gyrate at smaller radii then at a larger radii. An unbalanced particle flux in the poloidal direction produces a drift velocity called the diamagnetic drift velocity. The associated drift frequency is given by [16]

$$\omega_{*f} = -\frac{m}{r}\frac{v_f^2}{\omega_{cf}}\frac{1}{p_f}\frac{dp_f}{dr} \tag{3.43}$$

where m is the poloidal wave number and ω_{cf} and p_f are the cyclotron frequency and the pressure of the fast ions. If ω_{*f} is larger than the wave frequency, there is an effective inversion of the velocity space distribution function gradient $\partial f/\partial v$, so that

$$\frac{\omega - \omega_{*f}}{\omega}\frac{\partial f}{\partial v} > 0 \ , \tag{3.44}$$

which means that the free energy available from the fast ions can drive the mode.

3.6 Nonlinear Behaviour

Linearized MHD theory, as presented in section (2.3), describes the possible modes of magnetohydrodynamic oscillations, and the onset (and initial exponential growth) of these in the presence of available free energy, provided by e.g. super Alfvénic fast particles. However, as the perturbations grow, and eventually become comparable to the equilibrium quantities, i.e. when e.g. $B_1 \sim B_0$, the modes evolve into a nonlinear phase and the linearized approach

in section (2.3) brakes down. At this point, higher order terms need to be included to accurately describe the wave-particle interaction.

The nonlinear evolution of isolated instabilities was thoroughly analyzed in [18] and [19] by means of a simple 1D, electrostatic bump-on-tail model. Note that the highly simplified 1D geometry contains qualitatively the same physics features as more realistic, fully toroidal models [20][1], although quantitative results may well depend on the actual plasma equilibrium. In principle, two major regimes were detected: Away from threshold, i.e. when the linear drive γ_L from the fast particles by far exceeds the total damping rate γ_d from the background plasma, linear perturbations evolve into a quiescent nonlinear stage characterized by initial saturation of the mode amplitude and formation of phase space plateaus, followed by a gradual decay of the mode amplitude and the plateau width [21]. In the so called threshold regime,

$$0 < \gamma_L - \gamma_d \ll \gamma_L, \gamma_d \ , \tag{3.45}$$

on the other hand, there are four possible types of nonlinear evolution, and the linear perturbations may evolve into either of these depending on the collision frequency of the fast particles [18]: After the initial exponential growth the mode amplitude evolves nonlinearly and different evolution regimes can take place.

i. Saturation of the mode amplitude: If the collisionality is high enough, the mode amplitude saturates at a level that reflects the closeness to threshold.

ii. Modulation/pitchfork splitting: At somewhat lower collisionality, the mode develops closely situated sidebands, whose presence result in a characteristic splitting of the eigenfrequency.

iii. Spectral broadening: With even less collisions, the amplitude saturates but oscillates chaotically. The corresponding spectral signal consists of a broadening of the resonance lines.

iv. Bursting-type mode: With low enough collisionality, the mode develops highly persistent sidebands with time dependent frequencies and their own trapping regions in phase space (so called holes and clumps).

3.7 Particle Motion in Waves

Bursting type eigenmodes move radially within the plasma as their frequencies evolve in time. This motion can be calculated by recognizing that fast particles

[1] At least for TAEs, as long as the resonances are well separated in phase space and the frequencies remain close to those of the linear excitations.

trapped in the wave field move in synch with the mode localization radius. The particle velocity is represented as $\mathbf{v} = \mathbf{v}_{gc} + \mathbf{v}_L$, see section (2.1.2). For low frequency Alfvén waves, we will, however, consider only the gyrocenter motion. This can be motivated by looking at the resonance condition. For fast particles to be synchronized with the wave, they must satisfy

$$\omega = \langle \mathbf{k} \cdot \mathbf{v} \rangle_B \ , \tag{3.46}$$

where $\mathbf{k} = \mathbf{k}_\parallel + \mathbf{k}_\perp$, $\mathbf{v} = \mathbf{v}_\parallel + \mathbf{v}_D + \mathbf{v}_L$ and

$$\langle ... \rangle_B = \frac{1}{\tau_B} \int_0^{\tau_B} (...) \, \mathrm{d}t \ , \tag{3.47}$$

defines the bounceaverage. Taking $\langle \mathbf{k}_\perp \cdot \mathbf{v}_L \rangle_B \sim l\omega_c$, where $l \in \mathfrak{N}$, and since the Alfvén waves has $\omega \ll \omega_c$, we must have $l = 0$. We will therefore only consider gyrocenter motion and neglect the Larmor motion.

To derive an approximate expression for the radial motion of the wave, we limit ourselves to well passing particles, with $\kappa^2 \gg 1$, in a large aspect ratio tokamak, $\epsilon \ll 1$, for which the particle drifts are negligable. The condition (3.46) for wave-particle resonance becomes then

$$\omega(t) = k_\parallel \, v_\parallel \ , \tag{3.48}$$

where $\omega(t)$ is the wave frequency, $k_\parallel$ is given by (3.33) and $v_\parallel$ is given by (2.27). We assume that $k_\parallel$ is a function of radius only through the safety factor, meaning that all equations will be evaluated at the major radius of the torus $R = R_0$. Equation (2.27) for the parallel velocity then becomes

$$v_\parallel = \pm \sqrt{\frac{2}{m}(W - \mu B_0)} \ . \tag{3.49}$$

Since μ is an adiabatic invariant, the differentiation with respect to time of equation (3.48) results in

$$\dot{\omega} = \frac{dk_\parallel}{dr} v_\parallel \dot{r} + \frac{dv_\parallel}{dW} k_\parallel \dot{W} = \frac{mS}{qR_0 r} v_\parallel \dot{r} + \frac{k_\parallel}{M v_\parallel} \dot{W} \ , \tag{3.50}$$

where S is the magnetic shear, given by (3.40). The Hamiltonian of the system can be expressed as a sum of kinetic and potential energy. For particles trapped in the wave, the time rate of change of the potential energy is small, so we can assume that $\dot{W} \approx \dot{H} = \dot{E}$, where E is the total particle energy. We now wish to get an expression for $\dot{E}$ in terms of r.

In the absence of wave fields the toroidal angular momentum p_ζ is a constant of motion due to axisymmetry. In the presence of an external wave field,

depending on ζ, the axisymmetry will be broken and p_ζ and E are no longer constants of motion. However, it can be shown that

$$\dot{p_\zeta} - \frac{n}{\omega}\dot{E} = 0 \ , \tag{3.51}$$

holds. In a tokamak the potential ϕ is given by (3.29). In the presence of a wave the Lagrangian becomes

$$\mathcal{L} = \mathcal{L}_{unp} + \mathcal{L}_{pert} \ , \tag{3.52}$$

where $\mathcal{L}_{unp}$ is the unperturbed Lagrangian for a single charged particle (3.8) and $\mathcal{L}_{pert}$ is the perturbed Lagrangian due to the wave. In the expression (3.29) for the electrostatic potential ϕ the only dependence on ζ and t is in the propagation factor meaning that in the perturbed Lagrangian these dependences appear only in that form, so

$$\frac{\partial \mathcal{L}_{pert}}{\partial \zeta} = -\frac{n}{\omega}\frac{\partial \mathcal{L}_{pert}}{\partial t} \ . \tag{3.53}$$

The generalized momentum is given by (3.14) and using the Hamiltonian

$$H = p_i r^i - \mathcal{L} \ , \tag{3.54}$$

one obtains that the time derivative of energy is

$$\frac{dE}{dt} = -\frac{\partial \mathcal{L}}{\partial t} \ . \tag{3.55}$$

Furthermore,

$$\frac{dE}{dt} = \{E, H\} + \frac{\partial E}{\partial t} = \frac{\partial E}{\partial t} \ , \tag{3.56}$$

where $\{\cdot, \cdot\}$ is the Poisson bracket. We have shown in section (3.2) that

$$\frac{\partial \mathcal{L}_{unp}}{\partial t} = 0 \ . \tag{3.57}$$

Consequently

$$\frac{\partial \mathcal{L}_{pert}}{\partial \zeta} = -\frac{n}{\omega}\frac{\partial \mathcal{L}}{\partial t} = \frac{n}{\omega}\frac{dE}{dt} \ , \tag{3.58}$$

which by using the Euler-Lagrange equation becomes (3.51).

Using also the poloidal magnetic flux (3.2), which in a large aspect tokamak becomes

$$\psi \approx \int \frac{rB_0}{q}\,\mathrm{d}r \ , \tag{3.59}$$

we obtain

$$\frac{\partial \psi}{\partial r} = \frac{rB_0}{q} \ . \tag{3.60}$$

The toroidal angular momentum (3.16) can be expressed using the poloidal flux,

$$p_\zeta \approx MRv_\parallel - Ze\psi \ , \tag{3.61}$$

which after the bounce averaging and differentiation with respect to time becomes

$$\dot{\psi} = \frac{1}{Ze}\left(M\frac{d}{dt}\left\langle Rv_\parallel\right\rangle_B - \dot{p_\zeta}\right) \ . \tag{3.62}$$

To calculate the bounceaverage we use the θ-component of the gyrocenter motion (3.17b) to relate t to θ, where we neglect the drifts. For passing particles we have $\theta(0) = -\pi$ and $\theta(\tau_B) = \pi$ which leads to

$$\left\langle Rv_\parallel\right\rangle_B \approx 2\pi\frac{qR_0^2}{\tau_B} \ . \tag{3.63}$$

Taking the bounce time as given by (3.25), equation (3.63) becomes

$$\left\langle Rv_\parallel\right\rangle_B \approx R_0 v_{\parallel 0} \ . \tag{3.64}$$

Inserting (3.51), (3.60) and (3.64) into (3.62) yields the expression for $\dot{E}$, which substituted into (3.50) gives the radial drift of the particles as

$$\frac{\dot{r}}{r} = -\frac{\dot{\omega}}{\omega_c}\frac{m}{k_\parallel^2 r^2}\left(1 - \frac{m^2 S}{k_\parallel^3 r^2 qR}\frac{\omega}{\omega_c}\right)^{-1} \ . \tag{3.65}$$

4

Frequency Sweeping TAEs on MAST

The purpose of this thesis is the analysis of the frequency spectrum in Figure (4.1), which displays a set of peculiar perturbations observed in discharge 27177 at the spherical tokamak MAST. This discharge consists of a D-D plasma, heated by two beams of neutral deuterium with average particle energies 69 and 60 keV, respectively, which are injected into the plasma. MAST, see Figure (1.2), has a minor radius $a = 0.5$ m and a major radius $R_0 = 0.7$ m. The fact that the ratio of minor to major radius is large allows it to operate with a high ratio of particle to magnetic pressure, $\beta \sim \epsilon = a/R_0$, but also puts a lower limit on the toroidal magnetic field strength, due to the narrow inner leg. The low magnetic field strength in turn implies a low Alfvén velocity (2.53). The NBI injected fast particles, which have a much larger parallel than perpendicular energy, slow down due to collisions with thermal plasma particles and can fulfil the resonance condition (3.48). Consequently a mode can be excited when the parallel velocity of the fast particles matches the Alfvén velocity.

The spectrum in Figure (4.1) was obtained using the so called Mirnov coils, which measure the magnetic field outside the plasma vessel. The observed waves have frequencies of about 100 kHz, which is typical for the MHD instabilities in the TAE range at MAST. The perturbations can be detected at the edge of the plasma even when the amplitude is small. This is because the kHz range frequency leads to timescales much shorter then typical timescales for a change in the equilibrium magnetic field. The resulting electromagnetic fields induced in the Mirnov coils are then transformed to a frequency spectrum by means of the Fast Fourier Transform. Note that the TAEs are observed to evolve into bursting type modes, but the associated frequency sweeping has a preferred direction that changes in time. In this thesis we identify the TAEs

which evolve into the nonlinear bursting modes in Figure (4.1) and propose a possible mechanism behind the change in preferred direction which will be investigated further in a subsequent project.

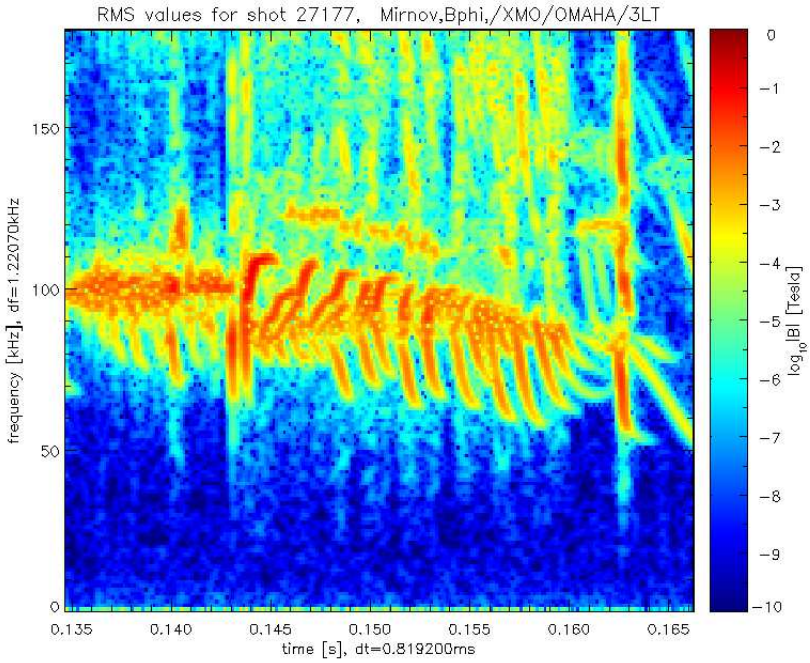

Figure 4.1: Frequency spectrum for discharge 27177 at MAST, measured by Mirnov coils at the plasma edge.

4.1 Method of Analysis

To identify the modes and later be able to describe the mechanism behind the continuous change of the preferred direction of the frequency sweeping in Figure (4.1), we use a combination of numerical modeling and analytical estimates. In this section, we present tools and expressions used to clarify the observed behaviour of the TAEs.

4.1.1 Mode Identification

To investigate the linear instabilities leading to the bursting nonlinear behaviour observed in Figure (4.1), one has to perform numerical modeling, with toroidal, elliptic and triangularity effects taken properly into account, as well

as a finite β and ϵ. The following three MHD codes have been used in the analysis:

i. HELENA: A Fortran 77 code that solves the Grad-Shafranov equation (3.7) for axisymmetric toroidal plasma equilibria, given inputs such as poloidal current flux, magnetic fields, etc. , as measured by diagnostic instruments at MAST. HELENA creates an output file that contains all relevant information about the instantaneous equilibrium, e.g. profiles for the MHD pressure and the safety factor and the Jacobian for a flux-type, straight field line coordinate system. This output file is needed for further modeling of the linear instabilities.

ii. CSCAS: A code that calculates the Alfvén continuum for a given plasma equilibrium. The input for CSCAS is the output file generated by HELENA.

iii. MISHKA: A code used to find eigenmodes of the linearized MHD equations (2.39). The code is designed to take as input the HELENA output file, described above, and a first guess for the eigenmode normalized frequency:

$$\lambda = \frac{\gamma R_0}{v_A(0)} \ , \tag{4.1}$$

where $\gamma = i\omega$, ω is the frequency of the mode and $v_A(0)$ is the Alfvén velocity (2.53) at the magnetic axis. The code then iterates and closes in on the nearest solution, which may be either a true eigenmode or the logaritmically singular continuum.

Note that CSCAS utilizes MISHKA to calculate the Alfvén continuum, by looking specifically for logarithmically singular solutions, satisfying the continuum condition $\omega^2 = \omega_A^2(r)$.

4.1.2 Description of Preferred Sweeping Directivity

The linear modes, which will be identified by the three MHD codes described in the previous section, are seen to quickly evolve into the bursting nonlinear regime (cf. Figure (4.1)). During the subsequent frequency sweeping, the modes are conveyed radially inside the plasma. To obtain a lowest order estimate of the radial transport, one may utilize that the trapped resonant particles are locked in the wave field of the mode. Hence the modes move in synch with the trapped particles, as their nonlinear frequencies evolve according to equation (3.65). The hypothesis is then made that the preferential direction of the frequency sweeping is such that the corresponding radial motion transports the mode towards higher values of the linear growth rate (3.42).

4.2 Results

First, HELENA, was run successfully, using inputs obtained from diagnostic instruments at the times $t = 144$ ms and $t = 158$ ms. (See Figs. (4.2) and (4.3) for examples of the safety factor profile and magnetic flux surfaces).

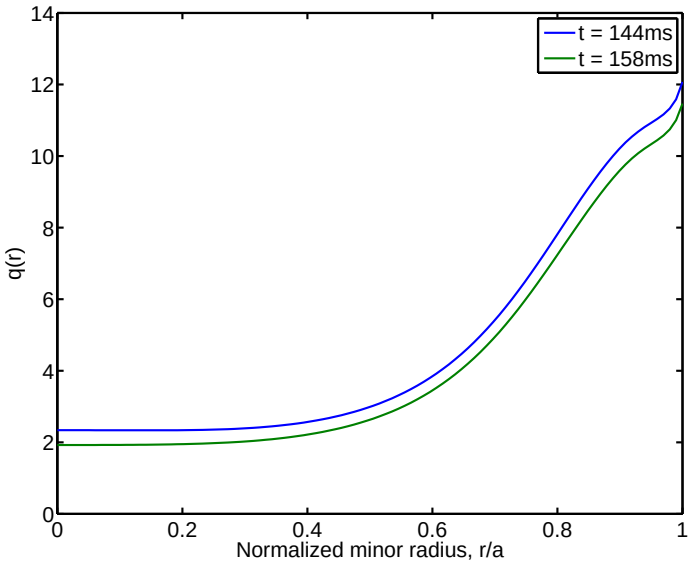

Figure 4.2: Safety factor profiles in discharge 27177, as calculated by the MHD equilibrium code HELENA.

Next, the Alfvén continuum was calculated at both times by means of CSCAS, in order to obtain an overview picture and provide first guesses of the eigenmode frequencies. The resulting plots are presented in Figure (4.4). Finally, the modes were identified as $n = 1$, global TAEs, with normalized frequencies $\lambda = 0.147i$ at time $t = 144$ ms and $\lambda = 0.125i$ at $t = 158$ ms, using MISKA. The normalized outputs from MISHKA were transformed to proper frequencies using the line averaged number density presented in Figure (4.5) and assuming a density profile of the form

$$n_e = n_0 \left(1 - \frac{r^2}{a^2}\right) \ , \tag{4.2}$$

where n_0 is the density at the magnetic axis. According to equation (4.1) the frequencies are $\omega = 130$ kHz at $t = 144$ ms and $\omega = 100$ kHz at $t = 158$ ms. Note that, the plasma rotation due to the injected fast particles gives rise to a Doppler shift and the difference at MAST is $10 - 20$ kHz between the measured frequencies from the Mirnov coils (cf. Figure (4.1)) and the

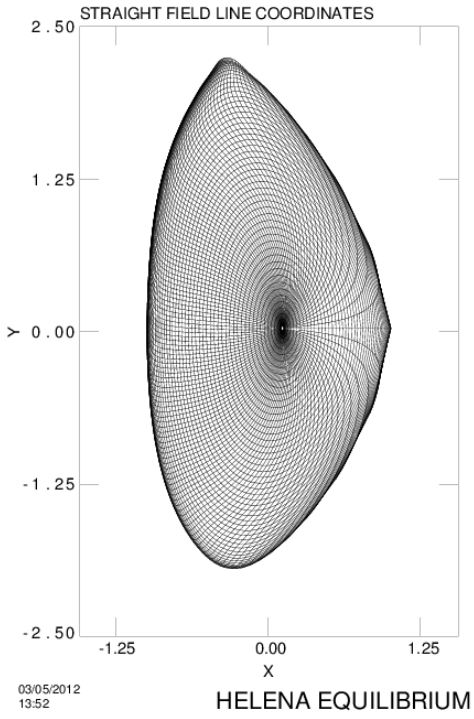

Figure 4.3: Magnetic flux surfaces at time $t = 144$ ms, as calculated by the MHD equilibrium code HELENA.

numerically calculated frequencies. Plots of the corresponding radial structures for the $n = 1$ TAEs are shown in Figure (4.6). Note that a zero reflection boundary condition was set at $r/a = 0.8$ in these runs in order to avoid a continuum resonance close to the plasma edge. Also note that the maximum amplitude of the global TAE in Figure (4.6) is at a larger radii at $t = 158$ ms then at $t = 144$ ms.

The nonlinear modes corresponding to the modes in Figure (4.6) evolve in time. The direction of the radial drift can be deduced using equation (3.65). We define the function $f(r)$ as

$$f(r) = \frac{m^2 S}{R_0 k_\parallel^3 r^2 q} \frac{\omega}{\omega_c} \ , \tag{4.3}$$

and the maximum of (f) is presented in Figure (4.7). Consequently, the direction of the radial drift is determined by the numerator in equation (3.65), since according to Figure (4.7) the denominator is approximately one throughout MAST.

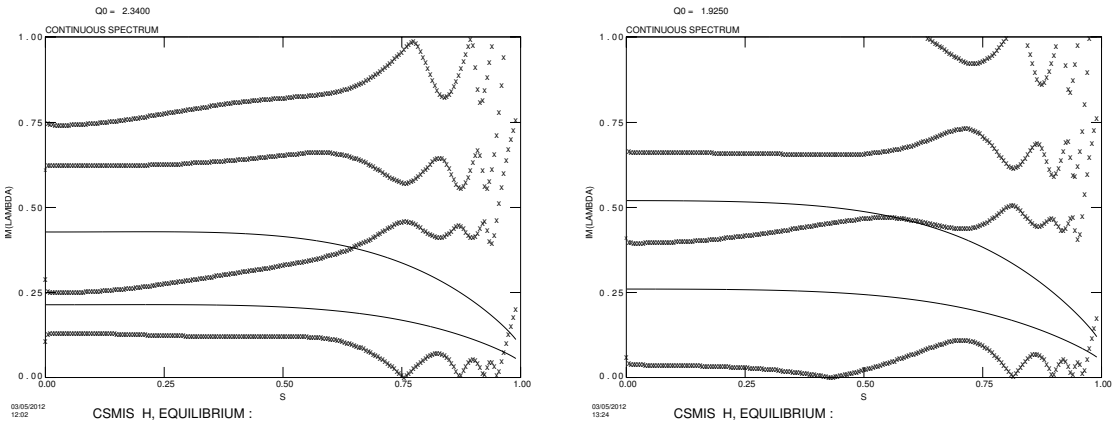

Figure 4.4: Alfvén continuum for $n = 1$ at time $t = 144$ ms (left) and $t = 158$ ms (right). The radial coordinate $s = \sqrt{\psi/\psi_{edge}}$ is the normalized poloidal flux and λ is the normalized frequency given by equation (4.1).

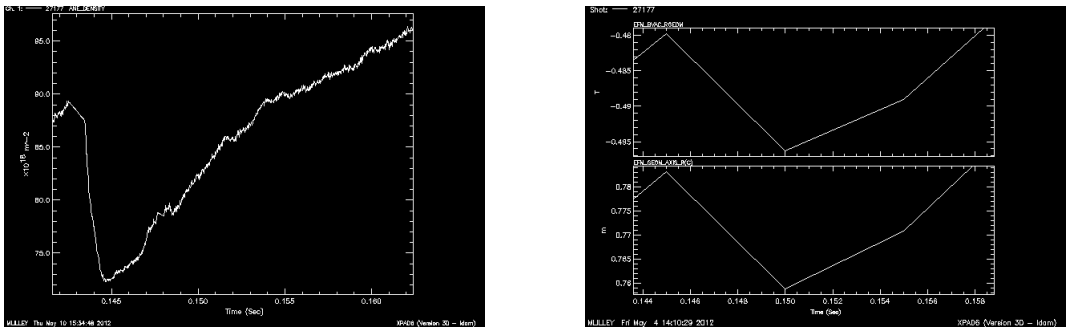

Figure 4.5: Line averaged number density for electrons (left), magnetic field (right top) and major radius (right bottom) at the magnetic axis.

Using values obtained from diagnostics at MAST at the time $t = 144$ ms we can calculate the Alfvén continuum in the cylindical limit, see Figure (4.8). Comparison with the eigenmode spectrum obtained from CSCAS, (cf. Figure (4.4)), leads us to the conclusion that the TAEs in Figure (4.6) consist of the poloidal mode numbers $m = 2$ and $m = 3$, which is confirmed by MISHKA. According to equation (3.65), the radial motion of upsweeping modes is then towards larger radii, while downsweeping nonlinear modes move towards smaller radii.

4.3 Conclusion and Discussion

The aim of this thesis has been to investigate the curious frequency sweeping exhibited in the spectrum presented in Figure (4.1), whose preferred directivity changes during the discharge. First, the equilibrium code HELENA was used to recreate the equilibrium conditions in MAST during the observation of the

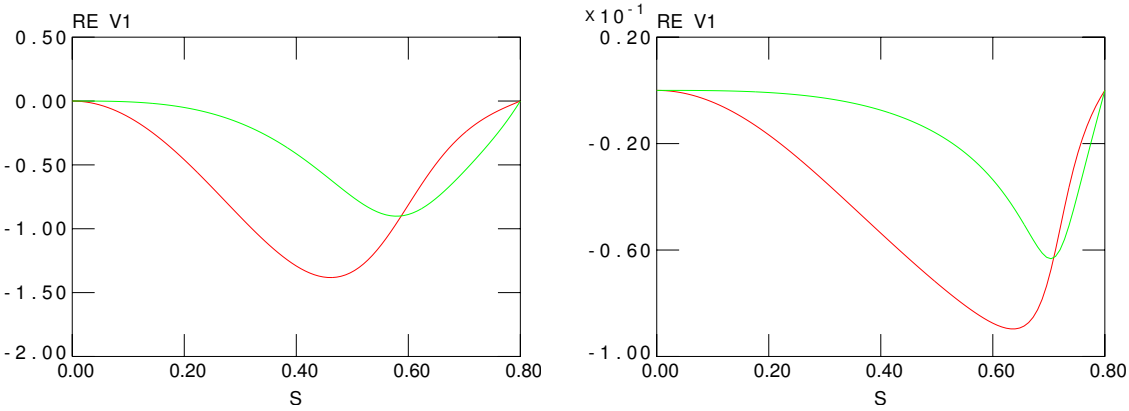

Figure 4.6: Radial structure for $n = 1$ eigenmodes at time $t = 144$ ms (left) and $t = 158ms$ (right). The amplitude of $V_1 \equiv sV_r$, where V_r is the radial component of the perturbed velocity, is shown as a function of the radial variable $s = \sqrt{\psi/\psi_{edge}}$.

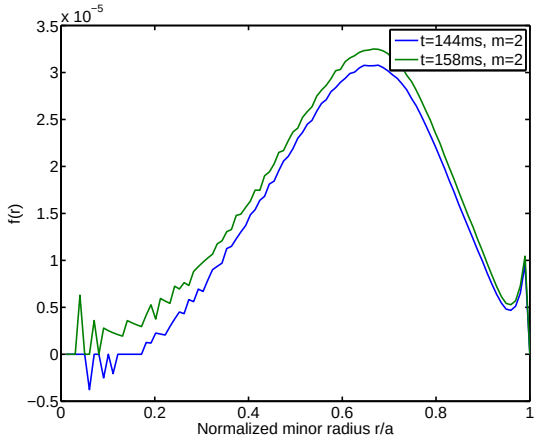

Figure 4.7: The maximum of $f(r)$ as given by equation (4.3).

modes. Then, using the linear codes CSCAS and MISHKA, we were able to show that there is an $n = 1$ eigenmode in the system with frequency $\omega = 130$ kHz at $t = 144$ ms and frequency $\omega = 100$ kHz at $t = 158$ ms. According to the theory of Section (3.5), this mode can be excited by the presence of energetic particles in the plasma, with a consecutive exponential growth of the linear perturbations when the linear growth rate due to the fast particles, γ_L, is slightly larger then the total damping in the plasma, γ_d. Nonlinear theory is then needed to describe the evolution of the modes which are observed to sweep in frequency (cf. Figure (4.1)) and thus correspond to the bursting modes.

The linear rate at which the wave amplitude initially increases due to the

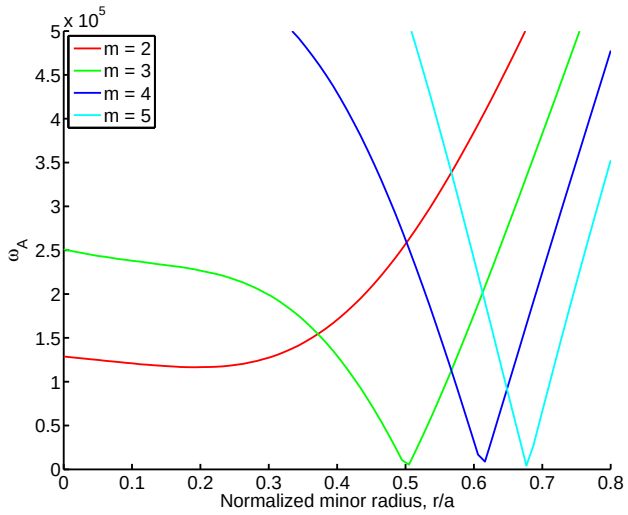

Figure 4.8: Crude estimate of the Alfvén continuum for $n = 1$ in the cylindrical limit, calculated using values obtained from diagnostics at MAST.

wave particle interaction is given by equation (3.42), and depends on the radial coordinate through the fast ion pressure profile. The original intention was to verify that during the considered time interval, (3.42) has a maximum close to, and between, the two linear mode excitation points at times $t = 144$ ms and $t = 158$ ms, respectively. If so, depending on whether the frequency sweeping corresponds to a movement towards or away from the maximum, the preferred sweeping directivity would be explained as mode amplitude enhancement or suppression due to increasing/decreasing γ_L. However, our investigation is not fully satisfactory for two reasons:

i. According to equation (3.65), there exist a radial motion of the modes as they sweep in frequency. Assuming a peaked γ_L with maximum between the mode excitation points, however, equation (3.65) suggests that the modes move in the "wrong" direction.

ii. We have not been able to verify that γ_L has a radial maximum between the mode excitation points, mainly because the measurements of the fast ion pressure profile were not readily avaiable from the MAST diagnostics. Furthermore, modeling of the fast ion profile by using the numerical code TRANSP would be too time consuming to be a part of this thesis.

Important to note, however, is that the assumptions behind the expression for the radial drift (3.65), are too crude to strictly apply to the MAST plasmas. In particular, $\epsilon \ll 1$ and $\beta \ll 1$ do not hold, and neither does the assumption that the fast ions do not deviate from the flux surfaces (in fact, NBI ions on MAST

have huge orbit widths, comparable to the minor radius). We thus conclude that equation (3.65) can not be used to investigate the sign or magnitude of the radial drift, but should be interpreted rather as an evidence that there exists a radial drift corresponding to the frequency sweeping. Hence, equation (3.65) constitues motivation to perform a more accurate, numerical work on the radial mode motion, which would quite likely reverse the predicted drift.

The linear MHD simulations revealed that the mode structure of the $n = 1$ mode on MAST is extremely global, see Figure (4.6), extending more or less from $r = 0$ to $r = a$. This has several implications: At first, it may appear as a show stopper, since the mode actually covers a large fraction of the tokamak cross section, and thus the entire normalized fast particle pressure gradient curve. However, it is natural to assume (as a first approximation) that the overall linear growth rate derives from the TAE gap surface, where the mode amplitude is maximum. This view, albeit another crude assumption made in order to simplify the analysis, is supported by the observation that a major part of the mode energy is concentrated close to the gap surface [14], in the so called inner layer. The global extension of the mode also means that it interacts with the fast particles during the entire poloidal revolution, even though the trajectories of NBI injected energetic particles at MAST deviate significantely from the magnetic flux surfaces.

The calculated frequencies for the TAEs match those in the frequency spectrum in Figure (4.1) very well when the Doppler shift is taken into account. When calculating the frequencies we used the line averaged number density for electrons, as given in Figure (4.5), which due to quasi-neutrality is the same as that for the deuterium ions. We also used the magnetic field strength at the magnetic axis and the location of the magnetic axis as given in Figure (4.5). Note that a dip is observed in all these plots (it is most pronounced in Figure 4.5) at time $t = 144$ ms, i.e. one of the two distinct times we are considering. This could be an indication that something happens that we do not consider in this model, and that may even be the reason for the change in frequency sweeping directivity. More likely, though, the dips are due to low frequency MHD activity which should not affect the TAE nonlinear mode evolution: As can be seen in the plot of the location of the geometric axis, the plasma moves first toward smaller radii and then toward larger radii as a response to the dip in electron density, which is very reminiscent of the $m = 1$ MHD instabilities. Obviously, these matters are interesting on their own, and should be investigated further to provide certain answers. Ideally for our purposes, though, a shot without this behaviour should be used to investigate the change in preferred frequency directivity. However, if one uses this shot it would be better to consider a later time than $t = 144$ ms (since that time is at the discontinuity of the line averaged number density), or simply show that the discontinuity does not affect the TAE sweeping.

What is left to be done in order to thoroughly investigate this behaviour is: First of all, the fast ion pressure profile needs to be modeled in order to obtain the shape of the linear growth rate at the considered time slices. For all we know, the frequency sweeping modes could in principle distort the shape of the linear growth rate and therefore affect the ensuing frequency sweeping. Second, more accurate, numerical work needs to be performed in order to determine the actual radial motion of the mode as its frequency sweeps. This is a formidable task on its own, which requires sophisticated modeling of the fast ion trajectories under the influence of a frequency sweeping wave. Finally, the proposed mechanism should be verified by full nonlinear simulations of the wave-particle interaction in a realistic geometry, using i.e. the numerical code HAGIS.

Bibliography

[1] U. S. Energy Information Administration, *www.eia.doe.gov*, May 10, 2012.

[2] J. Wesson, *Tokamaks*, Oxford University Press, Oxford, 3rd edition (2004).

[3] International Thermonuclear Experimental Reactor, *www.ITER.org*, May 10, 2012.

[4] W. W. Heidbrink and G. J. Sadler, *The Behavior of Fast Ions in Tokamak Experiments*, Nucl. Fusion **34** (4), 535 (1994).

[5] D. Anderson, M. Lisak, P. Johannisson and M. Marklund, *Basic Plasma Physics – Theory and Application*, Reproservice, Chalmers Tekniska Högskola, Gothenburg (2006).

[6] P. Helander, D. J. Sigmar, *Collisional Transport in Magnetized Plasmas*, Cambridge Monographs on Plasma Physics (2002).

[7] M. Lisak, *On the Linear and Quasi-Linear Theory of Thermonuclear Instabilities in a Tokamak Reactor*, Phys. Scripta **29** (1), 87 (1984).

[8] J. P. Freidberg, *Ideal magnetohydrodynamic theory of magnetic fusion systems*, Rev. Mod. Phys. **54** (3), 801 (1982).

[9] J. Candy, B. N. Breizman, J. W. Van Dam and T. Ozeki, *Multiplicity of low-shear toroidal Alfvén eigenmodes*, Phys. Lett. A **215**, 299 (1996).

[10] H. Goldstein, C. Pool, J. Safko, *Classical Mechanics*, 3Addison Wesley, 3rd edition (2002).

[11] M. N. Rosenbluth, H. L. Berk, J. W. Van Dam and D. M. Lindberg, *Mode structure and continuum damping of high-n toroidal Alfvén eigenmodes*, Phys. Fluids B **4** (7), 2189 (1992).

[12] H. L. Berk, J. W. Van Dam, Z. Guo and D. M. Lindberg, *Continuum damping of low-n toroidicity induced shear Alfvén eigenmodes*, Phys. Fluids B **4** (7), 1806 (1992).

[13] C. Z. Cheng, L. Chen and M. S. Chance, *High-n Ideal and Resistive Shear Alfvén Waves in Tokamaks*, Ann. Phys. **161**, 21 (1985).

[14] B. N. Breizman and S. E. Sharapov, *Energetic particle drive for toroidicity-induced Alfvén eigenmodes and kinetic toroidicity-induced Alfvén eigenmodes in a low-shear tokamak*, Plasma Phys. Control. Fusion **37**, 1057 (1995).

[15] T. Fülöp, M. Lisak, Ya I Kolesnichenko, D. Andersson, *Finite orbit width stabilizing effect on toroidal Alfvén eigenmodes excited by passing and trapped energetic ions*, Plasma Phys. Control. Fusion **38** (1996).

[16] S. E. Sharapov, *Fast Particle Driven Alfvén Eigenmodes in Tokamaks*, Fusion Science and Technology **57** 156 (2010).

[17] G. Y. Fu and J. W. Van Dam, *Excitation of the toroidicity-induced shear Alfvén eigenmode by fusion alpha particles in an ignited tokamak*, Phys. Fluids B **1** (10), 1949 (1989).

[18] M. K. Lilley, B. N. Breizman and S. E. Sharapov, *Destabilizing Effect of Dynamical Friction on Fast-Particle-Driven Waves in a Near-Threshold Nonlinear Regime*, Phys. Rev. Lett. **102**, 195003 (2009).

[19] M. K. Lilley, B. N. Breizman and S. E. Sharapov, *Effect of dynamical friction on nonlinear energetic particle modes*, Phys. Plasmas **17**, 092305 (2010).

[20] H. L. Berk, B. N. Breizman and M. S. Pekker, *Nonlinear Theory of Kinetic Instabilities Near Threshold*, Plasma Phys. Rep. **23** (9), 778 (1997).

[21] H. L. Berk, B. N. Breizman, J. Candy, M. Pekker and N. Petviashvili, *Spontaneous hole-clump pair creation*, Phys. Plasmas **6** (8), 3102 (1999).